



About Sections



Advei

STEM CELLS / Volume 33, Issue 5

Tissue-Specific Stem Cells |

## Undifferentiated State Induced by Rb-p53 Double Inactivation in Mouse Thyroid Neuroendocrine Cells and Embryonic Fibroblasts

Shunsuke Kitajima, Susumu Kohno, Atsushi Kondoh, Nobunari Sasaki, Yuuki Nishimoto, Fengkai Li, Mohammed Salah Abdallah Mohammed, Hayato Muranaka, Naoko Nagatani, ... [See all authors](#) ▾

First published: 19 February 2015

<https://doi.org/10.1002/stem.1971>

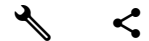
Cited by:7

### Abstract

Retinoblastoma tumor suppressor protein (RB) is inactivated more frequently during tumor progression than during tumor initiation. However, its exact role in controlling the malignant features associated with tumor progression is poorly understood. We established in vivo and in vitro models to investigate the undifferentiated state induced by Rb inactivation. *Rb* heterozygous mice develop well-differentiated thyroid medullary carcinoma. We found that additional deletion of *Trp53*, without change in lineage, converted these Rb-deficient tumors to a poorly differentiated type associated with high self-renewal activity. Freshly prepared mouse embryonic fibroblasts (MEFs) of *Rb*<sup>-/-</sup>; *Trp53*<sup>-/-</sup> background formed stem cell-like spheres that expressed significant levels of embryonic genes despite of lacking the ability to form colonies on soft agar or tumors in immune-deficient mice. This suggested that Rb-p53 double inactivation resulted in an undifferentiated status but without carcinogenic conversion. We next established *Rb*<sup>-/-</sup>; *N-ras*<sup>-/-</sup> MEFs that harbored a spontaneous carcinogenic mutation in *Trp53*. These cells (RN6), in an Rb-dependent manner, efficiently generated spheres that expressed very high



About Sections



genetic interaction between *Rb* and *p53* is a critical determinant of the undifferentiated state in normal and tumor cells. *STEM CELLS* 2015;33:1657–1669

## Introduction

RB and p53 tumor suppressor pathways are very frequently and often simultaneously aberrated in human cancers [1](#), [2](#). The combined inactivation of these proteins in mice can induce malignant neoplasia from a multitude of types of somatic cells [2](#), [3](#). Many of these tumors include those are not found in *Rb* only or in *Trp53* only-deficient mice [4](#), indicating a unique status of cells in which these two tumor suppressor pathways are simultaneously inactivated.

The inactivation in either of *Rb* or *Trp53* gene facilitates establishment of induced-pluripotent stem cells [5-8](#). However, the G2/M arrest and cell death were observed in human embryonic stem cells inactivated in all *RB* family members, which indicates their homeostatic roles in controlling stem cell activity [9](#). c-Myc is a representative target of RB, and c-Myc targeted germline might account for the similarities between embryonic stem cell and cancer cell transcriptome [10](#). NANOG interacts with CDC25A and CDK6 physically and functionally, which leads to short G1 phase that is most likely caused by attenuated activity of RB [11](#). *Trp53* transcription is maintained at low level in embryonic stem cells [12](#). These might be some of the cell cycle-dependent mechanisms of pluripotency [13](#). Conversely, the presence of the p53-mSin3a-HC transcription-suppressing complex on the *Nanog* gene promoter might be a cell cycle-independent mechanism by which p53 controls pluripotency [14](#). In addition, upon inactivation of Rb, E2Fs cooperate with Oct4 to exert positive feedback on Oct4-targeted genes [15](#). Moreover, Rb was directly implicated in the transcriptional control of *Sox2* and *Oct4* [16](#). These findings suggest that there is a significant linkage between the *RB-TP53* axis and embryonic stem cell-specific genes. Furthermore, the physical interactions between RB and a number of chromatin modifiers carrying LxCxE motif [17](#) implicate that RB inactivation has a genome-wide influence on the epigenetic changes required for obtaining pluripotency. In addition, much evidence indicates that RB plays pivotal roles in tissue stem cells and progenitor cells [13](#), [18](#). However, determining the functions of RB in these contexts is challenging because of the complicated cellular response to the loss of function of RB [19](#). For example, the germline loss of *Rb* results in increased intracellular signaling, DNA damage responses, and cellular senescence [19-22](#); this generated technical difficulties in addressing RB functions especially controlling undifferentiated state.



About Sections



In addition, the depletion of RB in a *Trp53*-null background allowed mouse embryonic fibroblasts (MEFs) to efficiently form stem cell-like spheres and express embryonic genes without affecting the cell cycle, cell viability, cellular senescence, or even tumorigenic activity. These two findings suggest that the inactivation of RB-p53, which is observed commonly in human cancers, might at least partially explain the mechanism underlying stem cell-like activities exhibited by cancer cell subpopulations. Therefore, we screened an FDA-approved drug library to identify agents that specifically attenuate the spherogenic activities exhibited by carcinogenic *Rb*-deficient *Trp53*<sup>mut</sup> fibroblasts. Taken together, these data suggest that determining the functions and targets of RB in a *Trp53*-null background might help identify novel targets for cancer therapy, particularly those that control malignant progression and recurrence.

## Materials and Methods

### Animals

*Rb* knockout mice were obtained from Dr. T. Jacks [23](#). *Trp53* knockout mice [24](#) were from RIKEN BRC (CDB0001K, [ja.brc.riken.jp](http://ja.brc.riken.jp), tsukuba, Japan). *Cdkn1* knockout mice [25](#) were from Drs. P. Leder and E. Hara. *Arf* knockout mice [26](#) were from Dr. Kamijo. All animals were handled in accordance with the guidelines of Kanazawa University.

### Immunohistochemical Analysis

Isolated thyroid tumors were fixed in 4% paraformaldehyde in phosphate buffered saline (PBS), and embedded in paraffin. Tissue sections (5  $\mu$ m) were stained with polyclonal antibodies to calcitonin (PA1-36049, Thermo Fisher Scientific, [www.thermofisher.com](http://www.thermofisher.com), Waltham, MA) or chromogranin A (ab15160, Abcam, [www.abcam.com](http://www.abcam.com), Cambridge, UK), or monoclonal antibody to Ki-67 (clone D3B5; Cell Signaling Technology, [www.cellsignal.com](http://www.cellsignal.com), Danvers, MA) or synaptophysin (clone SY38, Progen, [www.progen.de](http://www.progen.de), Heidelberg, Germany) using Dako Envision kit, and counterstained with hematoxylin. More than 300 cells were counted from three different fields at  $\times 40$  magnification for each sample.

### Thyroid Tumor Cell Preparation

To establish thyroid tumor cell lines, the tumors were carefully separated from thyroid gland by removing all surrounding tissues, minced with scissors, and suspended in Dulbecco's modified medium (DMEM) containing 300 units/ml collagenase, 100 units/ml hyaluronidase,



About Sections



Cells cultured under two-dimensional (2D) conditions (monolayer) were dissociated with trypsin-EDTA, filtered through a 40  $\mu\text{m}$  cell strainer, and then inoculated into 1% methylcellulose-containing  $\alpha$  modified Eagle's medium ( $\alpha$ MEM) supplemented with B-27 (Thermo Fisher Scientific, [www.thermofisher.com](http://www.thermofisher.com), Waltham, MA), 10 ng/ml human epidermal growth factor (EGF) (PeproTech, [www.peprotech.com](http://www.peprotech.com), Rocky Hill, NJ), and 10 ng/ml human basic fibroblast growth factor (bFGF) (PeproTech, [www.peprotech.com](http://www.peprotech.com), Rocky Hill, NJ), and without serum, at a density of  $2.5\text{--}5 \times 10^4$  cells on six-well-type ultra-low attachment well (E-Z BindShut II, AGC Techno Glass, [www.atgc.co.jp](http://www.atgc.co.jp), Shizuoka, Japan). After 7 day incubation, spheres were observed with the assistance of an inverted phase-contrast microscopy, and analyzed by BZ analysis software on BZ-9000 (Keyence, [www.keyence.co.jp](http://www.keyence.co.jp), Osaka, Japan) using hybrid cell counting module. Sphere-forming units were determined at a given day by counting cell aggregates larger than a given square micrometer surface area and with the ratio of the longest diameter and the shortest diameter ( $L/S$  ratio) less than 1.5 (spherical figure). Whole area in a dish was scanned by automated microscope, and sphere number per dish was calculated from tiled image data. For serial passage of sphere-forming cells, spheres were collected by centrifuge, and dissociated in Accumax (AM105, Innova Cell Technologies, [www.accutase.com](http://www.accutase.com), San Diego, CA) at 37°C for 15 minutes. The resultant cells were filtered through a 40  $\mu\text{m}$  cell strainer, and plated onto six-well-type ultra-low attachment well ( $2.5\text{--}5 \times 10^4$  per well).

## Cell Proliferation Assay

Cells ( $1.5 \times 10^5$ ) were seeded onto 35 mm diameter (D35) dishes. After 3 day incubation, the total number of cells in each dish was counted using a particle counter (Coulter Counter Z1, Beckman Coulter, [www.becjmancoulter.com](http://www.becjmancoulter.com), Brea, CA). This procedure was repeated every 3 days for two to three passages.

## RT-qPCR

Total RNA was isolated from cultured cells using TRIzol (Life Technologies) according to the manufacturer's instructions. A high capacity RNA to cDNA kit (Thermo Fisher Scientific, [www.thermofisher.com](http://www.thermofisher.com), Waltham, MA) was used to synthesize cDNA. In a 5  $\mu\text{l}$  reaction, the purified total RNA (200 ng) was reverse-transcribed at 37°C in the presence of random hexamer primers, and reaction products were diluted with 15  $\mu\text{l}$  of water. PCR was performed



About Sections



products was measured directly by monitoring fluorescence intensity on LightCycler 480 Instruments II (Roche, [www.roche.com](http://www.roche.com), Basel, Switzerland). Taqman probes used are as follows: *calcitonin/calcitonin-related polypeptide alpha* (*Calca*, Mm00801462\_m1), *achaete-scute complex homolog 1* (*Ascl1*, Mm03058063\_m1), *synaptophysin* (*Syp*, Mm00436850\_m1), *chromogranin A* (*Chga*, Mm00514341\_m1), *secretogranin II* (*Scg2*, Mm00843883\_s1), *solute carrier family 18 member 1* (*Slc18a1*, Mm00461868\_m1), *hypoxanthine guanine phosphoribosyl transferase* (*Hprt*, Mm01545399\_m1), *POU domain class 5 transcription factor 1* (*Pou5f1*, Mm03053917\_g1), *retinoblastoma 1* (*Rb1*, Mm00485586\_m1), and *SRY-box containing gene 2* (*Sox2*, Mm03053810\_s1). The relative level of gene expression was normalized using the level of *Hprt*.

## Generation of MEFs

Primary MEFs were prepared as described previously [28](#) from individual embryo of various genotypes, and maintained in  $\alpha$ MEM supplemented with 10% FBS. Primary MEFs were used each experiment before reaching 10 passages.

## Colony Formation Assay

Cells ( $1 \times 10^3$ ) were plated onto D100 dishes. After 14 day incubation, resultant colonies were visualized by Giemsa staining.

## RNA Interference

MISSION TRC shRNA target sets for mouse *Rb* (TRCN42543 and TRCN42544), mouse *Trp53* (TRCN12359 and TRCN12361), and negative control (Nontarget; SHC002) were purchased from Sigma-Aldrich ([www.sigmaaldrich.com](http://www.sigmaaldrich.com), St. Louis, MO). Generation and infection of lentivirus were performed according to the manufacturer's instruction.

## 3T3 Protocol

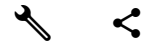
Cells ( $3 \times 10^5$ ) were plated in D60 dishes. After 3 days incubation, the total number of cells in each dish was counted using a particle counter, and  $3 \times 10^5$  cells were replated onto the D60 dishes. This procedure was repeated every 3 days for 16 passages [29](#).

## Immunoblotting

Immunoblotting of whole-cell lysates was performed as described previously [28](#) using antibodies to: Poly (ADP-ribose) polymerase (PARP) (#9542, Cell Signaling Technology,



About Sections



## BrdU Incorporation

Cells ( $1.5 \times 10^5$ ) were plated onto 0.1% gelatin-coated slides in six-well-type plate. After overnight incubation, cultured cells were incubated with 10  $\mu$ M BrdU for 20 minutes. Samples were stained using the BrdU Labeling and Detection Kit I (#11 296 736 001, Roche, [www.roche.com](http://www.roche.com), Basel, Switzerland) according to the manufacturer's instruction. Cell nuclei were counterstained with 4',6-Diamidino-2-Phenylindole, Dihydrochloride (DAPI), visualized by a fluorescence microscopy, and analyzed by BZ analysis software on BZ-9000 using hybrid counting module.

## TUNNEL Assay

Cells ( $1.5 \times 10^5$ ) were seeded onto 0.1% gelatin-coated slides in a six-well plate. After overnight incubation, apoptotic cells were assessed using In Situ Cell Death Detection Kit (#11 684 795 910, Roche, [www.roche.com](http://www.roche.com), Basel, Switzerland) according to the manufacturer's instruction. Cell nuclei were counterstained with DAPI and visualized on a fluorescence microscopy (AX1 ZEISS, [www.zeiss.com](http://www.zeiss.com), Oberkochen, Germany). For each experiment, cells treated with 0.1 mg/ml DNase I at 25°C for 10 minutes were used as positive control.

## Generation of Lentivirus

Mutant mouse *Trp53* cDNA derived from RN6 cells and wild-type mouse *Trp53* cDNA were cloned into pENTR (A10462, Thermo Fisher Scientific, [www.thermofisher.com](http://www.thermofisher.com), Waltham, MA) at BamHI and EcoRI site, sequenced by ABI 3130 sequencer, and then subcloned into pLenti6.3/V5-DEST (V533-06, Thermo Fisher Scientific, [www.thermofisher.com](http://www.thermofisher.com), Waltham, MA) using GATEWAY system. pLenti6.3/V5-HA-RB was made by transferring cDNA from pLXSB-HA-RB 21. Upon handling recombinant DNA, we strictly followed the National Institutes of Health guidelines. For lentivirus production,  $8 \times 10^6$  293T cells were transfected with 16  $\mu$ g of pLenti6.3/V5-LacZ or pLenti6.3/V5-HA-RB mixed with 12  $\mu$ g of RRE-pack and 4  $\mu$ g of VSVG-Re and in 46  $\mu$ g/ml polyethylenimine. After 48 hours incubation, the media containing lentivirus were collected, passed through a 0.45  $\mu$ m filter, and concentrated using polyethylene glycol.

## Soft Agar Assay

Cells ( $2.5 \times 10^4$ ) were dispersed and suspended in  $\alpha$ MEM containing 10% FBS and 0.33% agar and then mounted over a bottom layer of solidified  $\alpha$ MEM containing 10% FBS and 0.8% agar.





About Sections



*Rb*<sup>-/-</sup>; *Trp53*<sup>-/-</sup> MEFs, or RN6 cells transduced with pLenti6-LacZ or pLenti6-HA-RB using a lentivirus, suspended in  $\alpha$ MEM with Matrigel (BD Biosciences, [www.bdbiosciences.com](http://www.bdbiosciences.com), San Jose, CA) were inoculated subcutaneously into 6–8 weeks old male Kiyoshi Suzuki KSN/Slc immune-deficient mice (0.1 ml per site/animal;  $n = 4-8$ ) (Japan SLC, [www.jslc.co.jp](http://www.jslc.co.jp), Shizuoka, Japan). Tumors were weighed at 2 months after injection. The experiment using mice was carried out following institutional guidelines of Kanazawa University.

## Chemical Library Screening

FDA approved drug library (Enzo Life Science) containing 636 compounds was used for the screen. All chemicals were dissolved in Dimethyl sulfoxide (DMSO) at the concentration of 10 mg/ml and arranged in 96-well-type plate. RN6 cells were seeded on ultra-low attachment 96-well-type plate (1,600 cells/well), and incubated in serum-free  $\alpha$ MEM supplemented with 20 ng/ml bFGF, 20 ng/ml EGF, and B-27. The cells were incubated with 5  $\mu$ g/ml of the chemicals the library for 2 weeks, then analyzed by BZ analysis software on BZ-9000 using hybrid cell counting module. The effect of compounds was determined at a single data point on triplicate experiments. Each plate contained three negative control wells with DMSO alone, and three positive control wells with 5  $\mu$ g/ml atorvastatin.

## Statistical Analysis



Statistical significance for the number and size of spheres, relative mRNA expression, and cell growth were determined using unpaired Student's *t* test between two groups or one-way ANOVA followed by post hoc Tukey's test among more than three groups. Drug screening results were analyzed using one-way ANOVA followed by post hoc Dunnett's test. *p* values less than .05 were considered statistically significant.

## Result

### C Cell Tumor Phenotypes in Mice Deficient of Both Rb and p53

We reported previously that the thyroids of *Rb* heterozygous mice develop C cell adenoma or low grade C cell adenocarcinoma (thyroid medullary carcinoma). In addition, these tumors progress to the highly aggressive C cell adenocarcinoma when placed in a genetic background lacking *N-ras* 22, *Ink4a*, *Arf*, *Ink4a* and *Arf*, *Suv39h1* 21, or *ATM* 20 individually. This phenomenon



 About  Sections

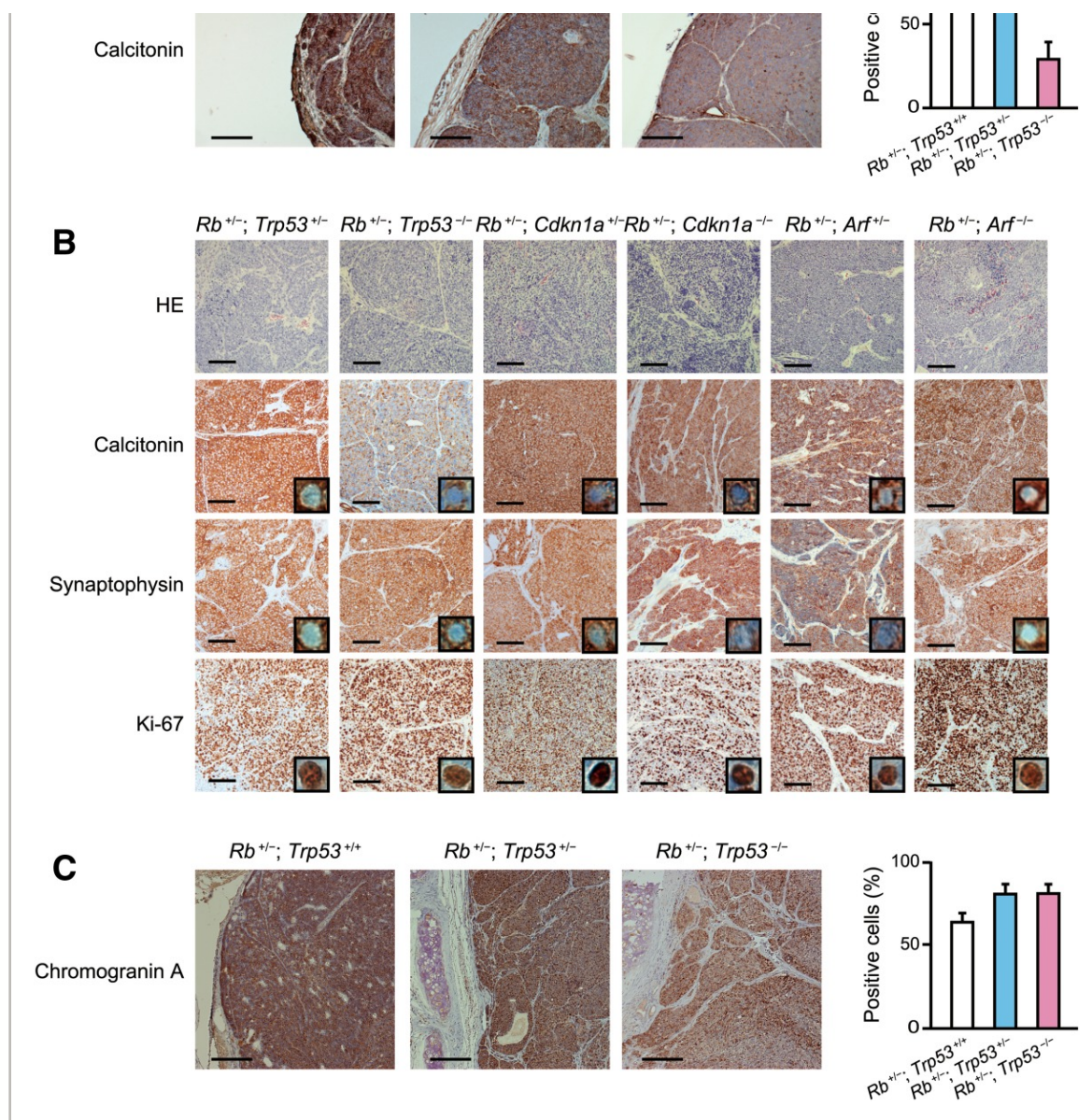


4, 30, *Rb* heterozygous mice in a *Trp53*<sup>-/-</sup> background were significantly shorter lived compared with those in a *Trp53*<sup>+/-</sup> or *Trp53*<sup>+/+</sup> background (Supporting Information Fig. S1) compared with *Rb* heterozygous mice in other genetic backgrounds that lack *Cdkn1a* (coding p21/Waf/Cip1) or *Arf* (Supporting Information Fig. S1). The observation and pathological examination revealed that *Rb*<sup>+/-</sup>; *Trp53*<sup>-/-</sup> mice had a shorter disease-free period compared to those of *Trp53*<sup>+/-</sup> or *Trp53*<sup>+/+</sup> background, which was attributed to accelerated pituitary carcinogenesis exactly as described previously 30. *Rb*<sup>+/-</sup>; *Arf*<sup>-/-</sup> mice showed shorter survival as compared to *Rb*<sup>+/-</sup>; *Arf*<sup>+/-</sup> mice, which also was attributed to accelerated pituitary carcinogenesis exactly as described previously 31. Macroscopic thyroid tumors were present in most of *Rb*<sup>+/-</sup>; *Trp53*<sup>-/-</sup> (mean age at observation: 4–5 months because of poorer survival) and *Rb*<sup>+/-</sup>; *Trp53*<sup>+/-</sup> mice (mean age at observation: ~8 months). In contrast, the tumors were typically microscopic in *Rb*<sup>+/-</sup>; *Trp53*<sup>+/+</sup> mice up to ~8 months of age, as reported previously 19-22, 32 (Fig. 1A). Nevertheless, some *Rb*<sup>+/-</sup>; *Trp53*<sup>+/+</sup> mice exhibited macroscopic thyroid tumors after 13–14 months. These findings suggest that the *Trp53* status affects the growth of Rb-deficient thyroid tumors.





About Sections



**Figure 1**

[Open in figure viewer](#) | [PowerPoint](#)

Phenotypes in thyroid neuroendocrine tumors developed in *Rb*-heterozygous mice of various genetic backgrounds. **(A)**: Immuno-staining of thyroid tumors developed in the indicated genotypes of mice with antibody to calcitonin. Columns represent average percentage of immuno-positive cells plus SD. More than 200 cells were observed in three to seven tumors of each genotype. \*,  $p < .05$  by one-way ANOVA followed by post hoc Tukey's test. **(B)**: Immuno-staining of thyroid tumors from the indicated genotype of mice with antibody



About Sections



Table S1). Surprisingly, however, calcitonin staining revealed marked differences between thyroid tumors isolated from mice with different genotypes (Fig. 1A, 1B). The thyroid tumors developed in  $Rb^{+/-}; Trp53^{+/-}$  mice stained 93.5% (mean)  $\pm$  6.4% (SE;  $n = 7$ ) positive for calcitonin; however, those developed in  $Rb^{+/-}; Trp53^{-/-}$  mice stained only 29.2%  $\pm$  9.7% ( $n = 4$ ) positive (Supporting Information Table S1). The thyroid tumors that developed in much older (13–14 months)  $Rb^{+/-}; Trp53^{+/+}$  mice were 82.9%  $\pm$  3.7% calcitonin-positive, excluding the possibility that the reduction in calcitonin levels in the thyroid tumors from  $Rb^{+/-}; Trp53^{-/-}$  mice was age dependent (Supporting Information Table S1). Calcitonin-positive or -negative cells were detected uniformly throughout the thyroid tumors in  $Rb^{+/-}; Trp53^{-/-}$  mice (Fig. 1A, 1B), excluding the possibility of heterogeneous clonality provided by calcitonin-negative cells. The thyroid tumors developed in  $Rb^{+/-}; Arf^{-/-}$ , and  $Rb^{+/-}; Cdkn1a^{-/-}$  mice also had a high frequency of calcitonin-positive cells (Fig. 1B).

C cell tumors are categorized as neuroendocrine tumors. Thyroid tumors of all examined mice including  $Rb^{+/-}; Trp53^{+/-}$ ,  $Rb^{+/-}; Trp53^{-/-}$ ,  $Rb^{+/-}; Arf^{-/-}$ , and  $Rb^{+/-}; Cdkn1a^{-/-}$  stained positive for the neuroendocrine lineage marker synaptophysin (Fig. 1B). In addition, thyroid tumors of  $Rb^{+/-}; Trp53^{-/-}$ ,  $Rb^{+/-}; Trp53^{+/-}$ , and  $Rb^{+/-}; Trp53^{+/+}$  mice were all positive for another neuroendocrine lineage marker chromogranin A at the similar level (Fig. 1C). Therefore, we concluded that the homozygous deletion of *Trp53* did not induce a lineage change from the neuroendocrine origin of tumors in Rb-deficient mice, but induced significant degree of dedifferentiation (loss of calcitonin) within the same lineage of cells.

## Stem Cell-Like Activities in Rb and p53-Deficient C Cells

We next isolated tumors from thyroid, derived cells after digestion by collagenase and hyaluronidase, and cultured them under 2D or suspension culture conditions. Cells freshly derived from tumors developed in  $Rb^{+/-}; Trp53^{-/-}$  mice ( $n = 6$ ) grew faster than did those from  $Rb^{+/-}; Trp53^{+/-}$  mice ( $n = 6$ ) under 2D culture condition. Cells derived from a comparatively bigger tumor developed in an  $Rb^{+/-}; Trp53^{+/+}$  mouse grew more slowly compared with other cells (Fig. 2A). Surprisingly, only cells from  $Rb^{+/-}; Trp53^{-/-}$  mice ( $n = 6$ ) exhibited significant sphere-forming activity when cultivated on ultra-low attachment wells in serum-free media supplemented with EGF, bFGF, and B-27 (Fig. 2A). Spheres derived from  $Rb^{+/-}; Trp53^{-/-}$  mouse thyroid tumor cells showed significant level expression of *Sox2* and *Pou5f1* (Fig. 2B). Strikingly even under 2D culture conditions, thyroid tumor cells from  $Rb^{+/-}; Trp53^{-/-}$  and  $Rb^{+/-}; Trp53^{+/-}$  mice expressed significant level of *Pou5f1*, and tumor cells from  $Rb^{+/-}; Trp53^{-/-}$  mice under 2

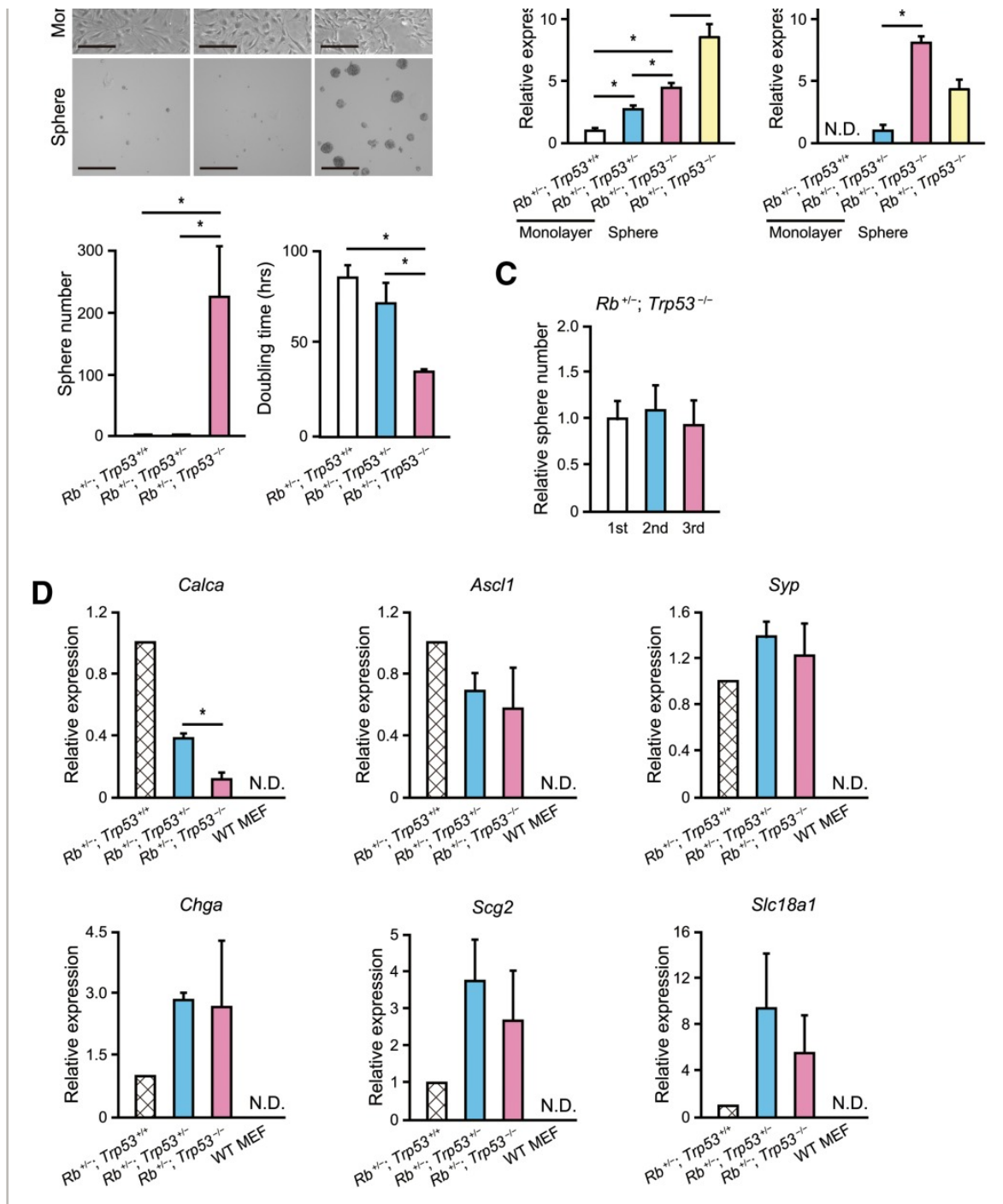


 About     Sections





About Sections



**Figure 2**

[Open in figure viewer](#) | [PowerPoint](#)

Behaviors in thyroid neuroendocrine tumors developed in *Rb*-heterozygous mice of various *Trp53* backgrounds. **(A)**: Cells derived from thyroid tumors



About Sections



when compared with that expressed in wild-type MEFs (Fig. 2B). Moreover, consistent with immunohistochemical staining result, synaptophysin (*Syp*) was expressed in thyroid tumors from  $Rb^{+/-}; Trp53^{-/-}$  and  $Rb^{+/-}; Trp53^{+/-}$  mice at a comparable level (Fig. 2D). We also examined the expression of other endocrine lineage markers. The expression levels of *chromogranin A* (*Chga*), *secretogranin II* (*Scg2*), and *solute carrier family 18* (vesicular monoamine transporter) *member 1* (*Slc18a1*) were not different in tumor cells between  $Rb^{+/-}; Trp53^{-/-}$  and  $Rb^{+/-}; Trp53^{+/-}$  mice, however were lower in a tumor from a *Trp53* wild-type mouse. Since the chance to derive  $p53^{+/+}$  C cell tumor is low, we could not further examine other  $Rb^{+/-}; p53^{+/+}$  mice. However, the levels of *Chga*, *Scg2*, and *Slc18a1* in all tumor cells were much higher than those expressed in wild-type MEFs. In non-neuroendocrine lineage markers, we tested *CD45*, *thyroglobulin*, and *solute carrier family 18 member 2*; they were all negative in any of thyroid tumor cells (data not shown).

In summary, except calcitonin, most of neuroendocrine lineage makers were maintained in deficient thyroid tumors regardless of the *Trp53* status. These findings exclude the possibility that p53 deficiency induced downregulation of *calcitonin* expression due to a lineage change. These findings further suggest that the change in differentiation status of neuroendocrine tumors represented by calcitonin status well correlated with self-renewal activity. Loss of calcitonin could be a stem cell marker for medullary thyroid cancers. Our results also indicate that only the homozygous loss of *Trp53* allowed Rb-deficient thyroid neuroendocrine cells to exhibit strong stem cell-like activity. Based on these findings, we further investigated the genetic interaction between *Rb* and *Trp53* during the induction of undifferentiated state.

## Behaviors of MEFs Lacking Both Rb and p53

We next generated mice homozygously lacking both *Rb* and *Trp53*. As reported previously [3], these mice exhibited lethality before around embryonic day (E) 14.5 (data not shown). We demonstrated previously that additional deletion of *N-ras*, *Ink4a*, *Arf*, or *Suv39h1* genes attenuated the resistance of  $Rb^{-/-}$  MEFs to senescence [21]. MEFs freshly derived from  $Rb^{+/-}; Trp53^{-/-}$  and  $Rb^{-/-}; Trp53^{-/-}$  E12.5 embryos exhibited significant resistance to cellular senescence when plated at a low density ( $1 \times 10^3$  cells per D100 dish) (Fig. 3A). In addition, Rb depletion by means of shRNA had no significant additional effect on the colony formation by MEFs derived from a *Trp53*-null embryo in a setting that Rb was efficiently depleted (refer Fig. 4B for the efficiency of knockdown) (Fig. 3B). Upon cell proliferation assay according to the 3T3 protocol,  $Rb^{+/-}; Trp53^{-/-}$  and  $Rb^{-/-}; Trp53^{-/-}$  MEFs exhibited highly similar cell proliferation





About Sections



cell proliferation, senescence, and cell death in a type 1a background.



About Sections

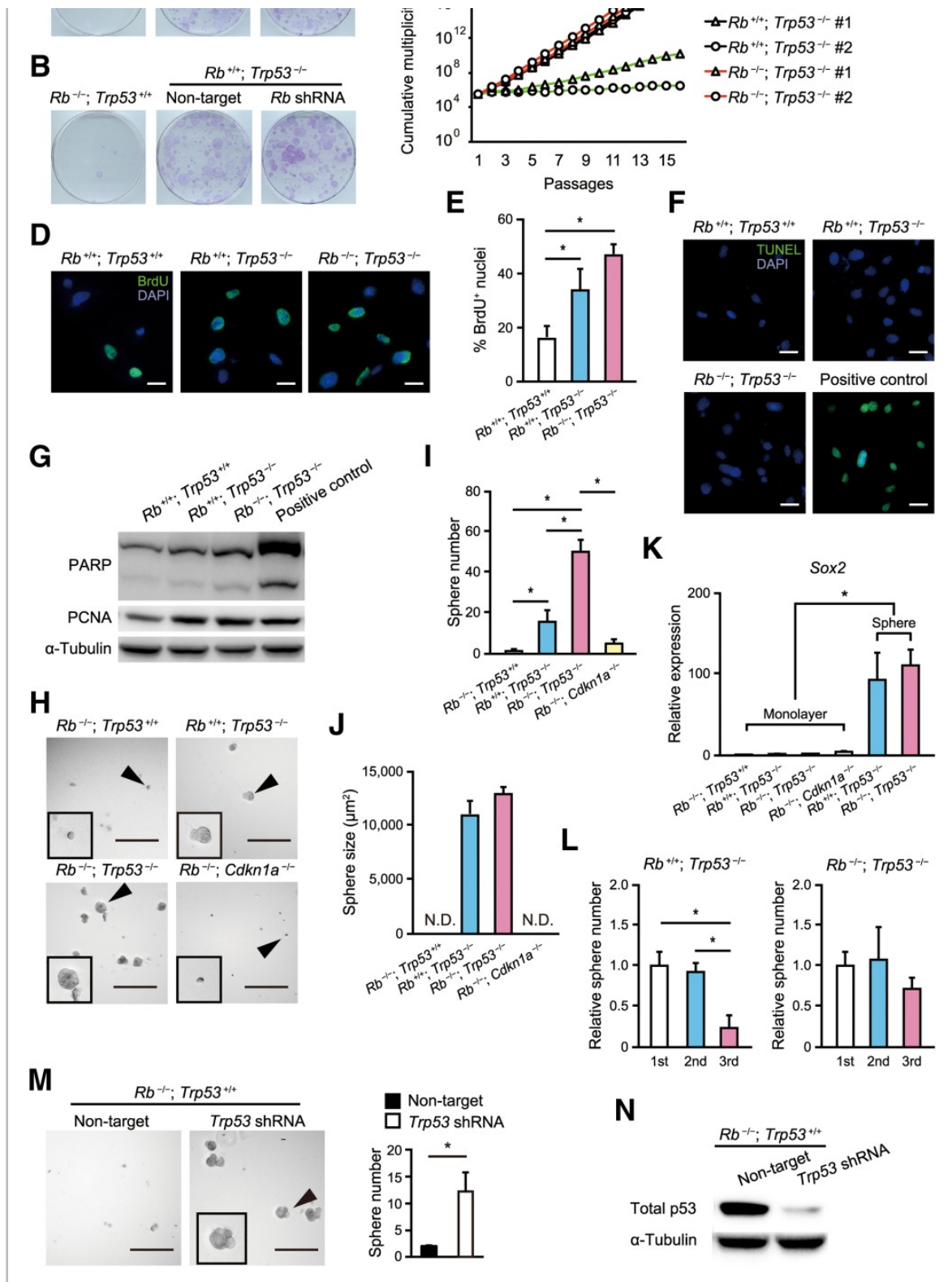
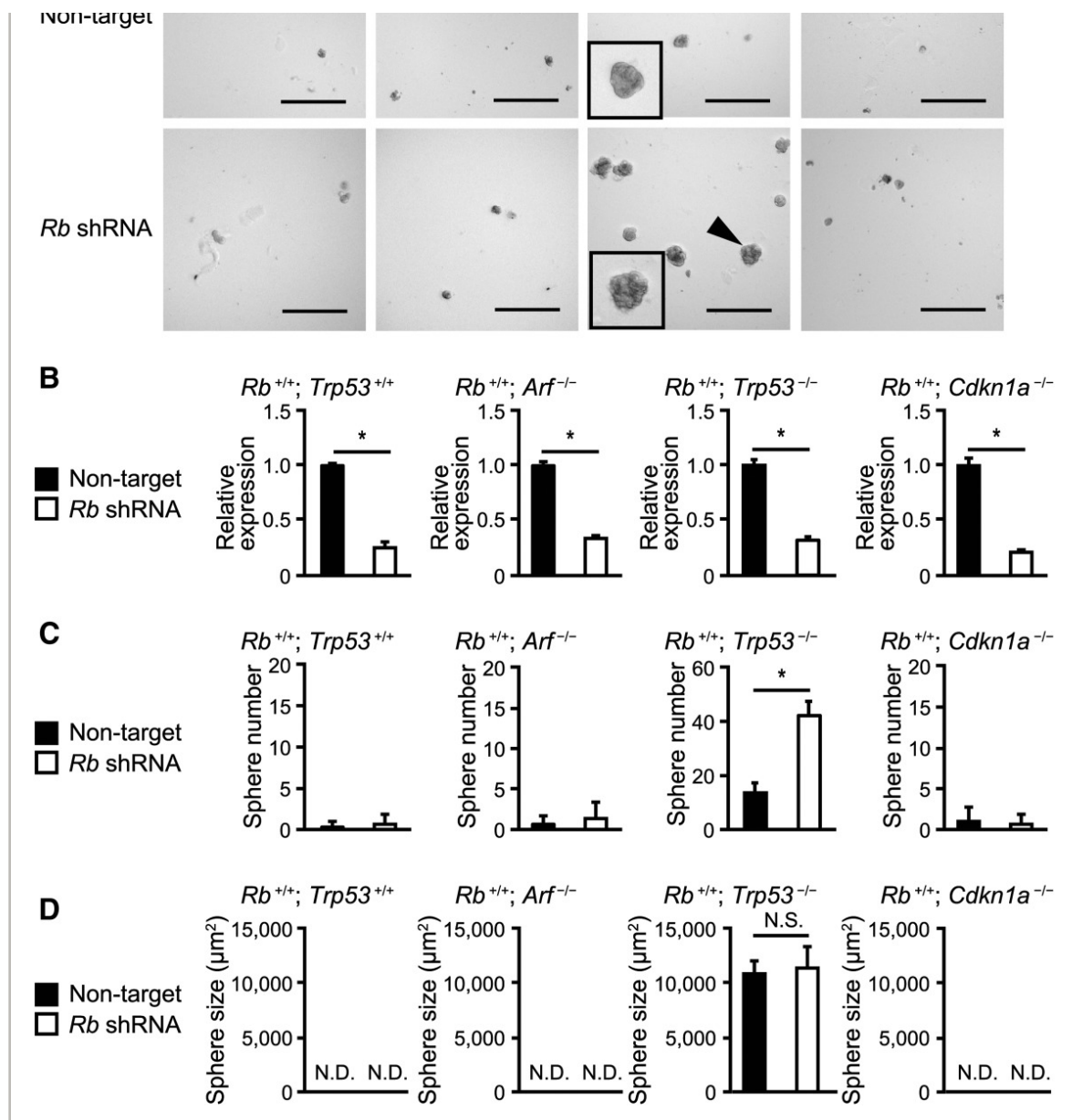


Figure 3





About Sections



**Figure 4**

[Open in figure viewer](#) | [PowerPoint](#)

Behaviors in mouse embryonic fibroblasts (MEFs) of various genetic backgrounds after Rb depletion. **(A)**: Sphere assay of the indicated genotype of MEFs transduced with the indicated shRNA. Scale bar = 200  $\mu\text{m}$ . **(B)**: Efficiency of Rb knockdown was assessed by RT-qPCR. \*,  $p < .05$  by Student's  $t$  test. **(C)**: Quantitative assessment of frequency (larger than 3,000  $\mu\text{m}^2$  surface area and less than 1.5  $L/S$  ratio), and **(D)** size of spheres ( $n = 3$ ). \*,  $p < .05$  by



About Sections




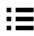
cell dedifferentiation status, we hypothesized that the *Trp53* status might play a crucial role in determining the stem cell-like features of *Rb*-deficient MEFs. Both *Rb*<sup>-/-</sup>; *Trp53*<sup>-/-</sup> and *Rb*<sup>+/+</sup>; *Trp53*<sup>-/-</sup> MEFs formed stem cell-like spheres in serum-free culture medium that was supplemented with EGF, bFGF, and B-27 (Fig. 3H). However, *Rb*<sup>-/-</sup>; *Trp53*<sup>-/-</sup> MEFs formed spheres much more efficiently than did *Rb*<sup>+/+</sup>; *Trp53*<sup>-/-</sup> MEFs (Fig. 3I). Additional deletion of *Cdkn1a*, a downstream gene of *Trp53* and encodes p21, only slightly induced sphere formation suggesting that the function of p53 in suppressing spherogenesis in an *Rb*-null background is largely independent of p21 function (Fig. 3I). The mean sphere size of *Rb*<sup>-/-</sup>; *Trp53*<sup>-/-</sup> and *Rb*<sup>+/+</sup>; *Trp53*<sup>-/-</sup> MEFs was not significantly different (Fig. 3J). Moreover, *Sox2* levels were not significantly different between *Rb*<sup>-/-</sup>; *Trp53*<sup>-/-</sup> and *Rb*<sup>+/+</sup>; *Trp53*<sup>-/-</sup> spheres (Fig. 3K). *Pou5f1* was not detected in spheres derived from these MEFs (data not shown).

Importantly, the activity to form spheres in *Rb*<sup>-/-</sup>; *Trp53*<sup>-/-</sup> MEFs were completely maintained for at least three passages, however, importantly, that in *Rb*<sup>+/+</sup>; *Trp53*<sup>-/-</sup> MEFs decreased after passage 3 (Fig. 3L). These findings suggest that *Rb*-deficiency sustains the ability to form spheres in a *Trp53*-null background. We confirmed that p53 depletion was sufficient to induce spheres in *Rb*-deficient cells (Fig. 3M, 3N). Most importantly, *Rb*<sup>-/-</sup>; *Trp53*<sup>-/-</sup> MEFs were unable to form colonies in soft agar assay or to initiate tumors when inoculated into KSN/Slc immunodeficient mice (data not shown). This suggests that these cells did not acquire stem cell-like activity as a consequence of carcinogenic changes.

## Rb Depletion Increases the Frequency of Sphere Formation in *Trp53* Null MEFs

We next depleted *Rb* in MEFs lacking *Trp53*, *Arf*, or *Cdkn1a*. *Rb* depletion significantly increased the frequency of sphere formation only in *Trp53*<sup>-/-</sup> MEFs without affecting sphere size, but not in MEFs of other genotypes (Fig. 4A–4D). We confirmed that *Rb* was significantly depleted in the genotype of MEFs to a comparable level (Fig. 4B). These findings suggest that the *Rb* status directly determines the sphere-forming efficiency in a *Trp53*-null background. Furthermore, p21<sup>Cdkn1a</sup> (one of the most important cell cycle regulators in downstream of p53) or p19<sup>Arf</sup> deficiency did not compensate p53 deficiency regarding sphere formation upon additional *Rb* depletion, although p21<sup>Cdkn1a</sup> and p19<sup>Arf</sup>-deficient cells show faster proliferation rate under culture conditions similar to p53-deficient cells (data not shown). These findings again suggest a unique genetic interaction between *Rb* and p53 in driving undifferentiated state that is exerted most likely through cell cycle-independent mechanisms.



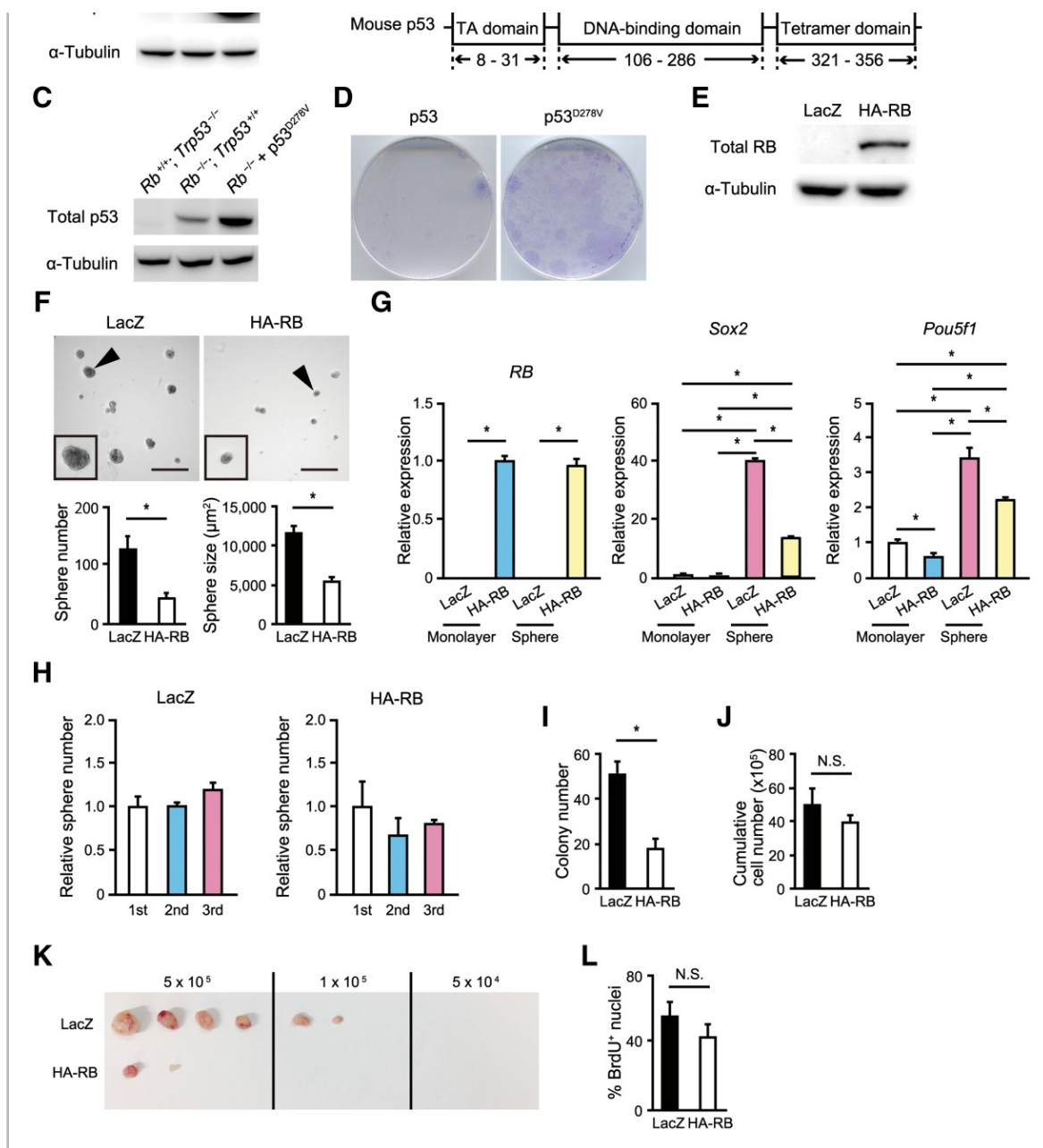
 About    Sections



parental cells; this line was named “RN6.” A screen of our collection of MEFs with various genotypes for the ability to form stem cell-like spheres detected RN6 but not the parental *Rb*<sup>-/-</sup>; *N-ras*<sup>-/-</sup> cells. Therefore, we next examined the *Trp53* status of RN6 cells; p53 protein was expressed highly (Fig. 5A). p53 is typically overexpressed in cancer cells harboring loss-of-function p53 mutations in the DNA-binding domain due to impairment of the negative feedback mechanism onto its abundance typically mediated by Mdm2. Indeed, we detected point mutation in the *Trp53* gene at the codon 278, which converted aspartate to valine (D278V) (Fig. 5B). This amino acid is located in the DNA-binding domain of p53, and corresponds to a region of human p53 that is a “hot spot” of carcinogenic mutations [35](#). We cloned *Trp53*<sup>D278V</sup> cDNA from RN6 cells, and transduced it into *Rb*<sup>-/-</sup> MEFs using a lentivirus, which induced colony formation (Fig. 5C, 5D). These findings suggest that D278V conversion affects p53 activity most probably by impairing its DNA binding activity. These findings again highlighted the role of *Trp53* for *Rb*-deficient MEFs to behave like stem cells.



About Sections



**Figure 5**

[Open in figure viewer](#) | [PowerPoint](#)

Behaviors in  $Rb^{-/-}; N-ras^{-/-}$  MEFs those spontaneously acquired loss-of-function mutation in  $Trp53$  (RN6 cells). **(A)**: Immunoblotting (IB) of the indicated proteins in the indicated cells. **(B)**: A missense mutation (D278V) identified in the DNA-binding domain of the  $Trp53$  gene in RN6 cells. **(C)**: Transduction of  $Trp53^{D278V}$  cDNA to the indicated genotype of MEFs, and



About Sections



derived from RN6 cells in which Rb had been overexpressed (Fig. 5C), interestingly, *Trp53* expression was downregulated in RN6 cells expressing RB under 2D culture conditions (Fig. 5G). Sphere-forming activity was slightly attenuated by RB overexpression during serial passage (Fig. 5H), which was associated with reduced colony formation efficiency in soft agar (Fig. 5I). However, there was no significant difference in cell proliferation between RB-overexpressing and control cells under 2D culture conditions (Fig. 5J), suggesting that RB status affects the behavior of RN6 cells specifically in 3D culture conditions and in the context of self-renewal.

Unlike freshly prepared *Rb*<sup>-/-</sup>; *Trp53*<sup>-/-</sup> MEFs, RN6 cells appeared to be carcinogenic when inoculated subcutaneously into KSN/Slc immune-deficient mice (Fig. 5K). We suspected the reasons why RN6 is carcinogenic unlike freshly prepared *Rb*<sup>-/-</sup>; *Trp53*<sup>-/-</sup> MEFs is because RN6 cells had undergone passages long enough for cells to overcome senescence and for carcinogenic cells to be selected. In addition, we assumed loss of *N-ras* helped *Rb*<sup>-/-</sup> MEFs to overcome senescence, gain rapid cell growth, and then encounter spontaneous mutation in *Trp53*. A serial titration experiment was then performed in vivo. When  $5 \times 10^5$  cells were inoculated, RB-overexpressing RN6 cells propagated in immune-deficient mice at only 25% of the levels of control (Lac Z) cells (Fig. 5K). Measurement of the tumor mass of samples excised from immune-deficient mice that were inoculated with  $5 \times 10^5$  cells suggested that RB exerts anti-“cancer initiation” effects beyond its impact on tumor size (Fig. 5K). Furthermore, when  $10^5$  cells were inoculated, RB-reconstituted RN6 cells had no chance to propagate, while control cells were still able to propagate at 50% (Fig. 5K). However, BrdU incorporation was not significantly different between control and RB-reconstituted RN6 cells (Fig. 5L). These findings suggest that RB exerts “cell cycle-independent” function to suppress cancer initiation.

## Characterization of RN6 Cells on FDA-Approved Drug Library Screening

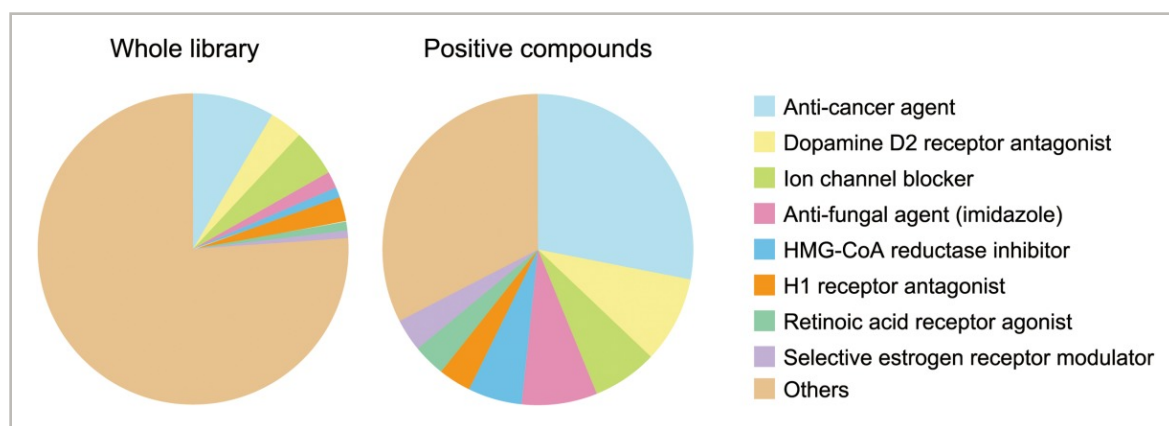
To further characterize RN6 cells, we screened an FDA-approved drug library that contains 636 drugs to identify chemicals that suppress sphere formation in RN6 cells. Fourteen percent of drugs (89 of 636) in the library suppressed sphere formation significantly (reducing sphere formation to less than 33% of vehicle-treated cells) at a dose of 5  $\mu$ g/ml. These 89 drugs were then classified according to their efficacy (Supporting Information Table S2; Fig. 6). As expected, many of anticancer agents were scored positive (25/54), while we noticed particular classes of drugs those were not categorized as anticancer drugs were scored positive at the



About Sections



The dopamine D2 receptor antagonists included thioazine (1-(2-(2-(2-methylpiperidin-2-yl)ethyl)-2-methylsulfonylphenothiazine) that had been reported to suppress cancer stem cells specifically [36](#). In addition, retinoid receptor agonists attenuate stem cell-like gene expression profile in breast cancer stem cells [37](#). Azole antifungal agents and HMG-CoA reductase inhibitors commonly target cholesterol biosynthesis pathway [38](#). These findings suggest that RN6 cells that acquired undifferentiated state following p53 mutation and exhibit stem cell-like activity in an Rb-dependent manner are sensitive to specific groups of drugs, including agents those had been demonstrated to be therapeutically effective against cancer stem cells.



**Figure 6**

[Open in figure viewer](#) | [PowerPoint](#)

Screen of 636 FDA-approved drug library searching for chemicals those suppress spherogenic activity of *Rb*-homozygous mouse embryonic fibroblasts harboring a loss-of-function mutation in *Trp53* (RN6 cells). Occupancy of the indicated category of drugs in the whole library (636 drugs) (left). Occupancy of the indicated category of drugs in 89 positively scored drugs that reduced sphere formation by RN6 cells to <33% of vehicle (DMSO)-treated cells with statistical significance ( $n = 3$ ;  $p < 0.01$  by Dunnett's test) (right). Abbreviation: HMG-CoA, hydroxymethylglutaryl-CoA.

[Caption](#) ▾





About Sections



lacking both *Rb* and *Trp53*; these were not observed in tissues lacking one of them individually 18. Similarly, as above-mentioned, Rb-p53 double inactivation generates unique types of tumors in mice that were not found in those deficient of one of them individually 4. For instance, the conditional knockout of Rb directed by mouse mammary tumor virus promote driven cre recombinase allowed mice to develop luminal B-type breast cancers; however, additional inactivation of p53 converted this type to a basal-like type 39. Indeed, RB and p53 are >70% and >90% inactivated in human basal-like breast cancers, respectively 40, 41. This suggests that RB and p53 are inactivated simultaneously in >60% of this type of cancer. Basal-like type breast cancers are proposed to be stemmed from the luminal progenitor cells common with luminal-like types 42. Therefore, these findings suggest that the status of p53 significantly affects the way that RB controls differentiation status in mammary epithelial cells. A similar relationship was observed in human soft tissue sarcomas and mouse models: well differentiated sarcomas that developed in p53-deficient mice were converted to undifferentiated pleomorphic sarcomas upon the additional inactivation of Rb 43. Conversely Rb depletion from *Trp53*-null osteosarcoma shifted tumor spectrum to hibernoma 44 suggesting a certain role of Rb in the fate decision of cells. Furthermore, the somatic loss of *Trp53* in lung epithelial cells was sufficient to generate hyperplasia or adenocarcinoma. Although the somatic loss of Rb in the same setting did not induce any lesions, the simultaneous loss of these genes induced small cell lung cancer 45, 46. These findings allow to hypothesize that the inactivation of RB in a *Trp53*-deficient background induces dedifferentiation and/or change in cell fate depending on the cellular context and that this occurs at least partially in a cell cycle-independent manner.

The number of malignancies that require RB inactivation for their initiation is unexpectedly limited. In most cancers, including breast, prostate, bladder, esophageal, hepatocellular carcinoma, glioma, and chronic myelogenous leukemia, RB is inactivated almost invariably during their progression 47. In addition, an undifferentiated developmental gene signature is often associated with the progression of these cancer cells 48. Therefore, although typically cancer stemness could be attributed to their origination in a tissue stem or progenitor cell, it could also be an activity that is de novo acquired or regained during tumor progression. This hypothesis led us to assess the functions of RB during tumor progression. Although the pathways activated by RB deficiency during tumor progression might provide critical targets for controlling the malignant behavior of cancers, previous studies failed to elucidate its clinical significance and molecular mechanism because of a lack of appropriate experiments.





About Sections



subpopulations. Based on the results of this study, we are currently identifying RB target genes in *Trp53*<sup>-/-</sup> mouse soft tissue sarcoma cells, *Trp53*<sup>-/-</sup> mouse mammary epithelial cells, and *Trp53*<sup>-/-</sup> mouse prostate epithelial cells in the context of sphere formation. These studies already identified that RB suppresses the undifferentiated state of cancer cells by regulating inflammation-related cytokines and chemokines, the glycolytic pathway, and the cholesterol biosynthesis pathway.

## Conclusions

This work demonstrated that the RB-p53 genetic interaction is a critical determinant in stem cell-like activities in normal and cancer cells. We also demonstrated that the function of RB to control undifferentiated state is mechanistically separable from that to control cell cycle. We further proposed that determination of RB targets in p53-inactivated cells in the context of tumor progression might provide a great opportunity to discover novel tools to control malignant progression of cancers.

## Acknowledgments

We thank Drs. T. Jacks, T. Kamijo, P. Leder, and T. Tanaka for providing materials, Drs. Asano and Kamimura for assistance in animal experiments, Dr. A. Yoshida for assistance in drawing survival curve, and all the colleagues in Takahashi laboratory for valuable discussion. This work was supported by Funding Program for Next Generation World-Leading Researchers (NEXT) C.T., Grant-in-Aid for Scientific Research (MEXT) to C.T., S.Kitajima, and N.S., Astellas Foundation for Research on Metabolic Disorders, Takeda Science Foundation, Naito Foundation, Daiichi-Sankyo Foundation for Life Science, NOVARTIS Foundation (Japan) for Promotion of Science, and Hokkoku Foundation for Cancer Research to C.T., and Hokuriku Bank Research Grant for Young Scientists to S.Kitajima. S.Kitajima thanks Strategic Young Researcher Overseas Visit Program for Accelerating Brain Circulation for fellowship.

## Author Contributions

S.Kitajima: conception and design, collection and assembly of data, data analysis and interpretation, manuscript writing, and financial support; S.Kohno: conception and design, collection and assembly of data, data analysis and interpretation, and manuscript writing; A. F.L., M.S.A.M., N.N., M.S., and Y.K. collection and assembly of data; N.S.: construction of



 About    Sections



---

The authors indicate no potential conflicts of interest.

**Supporting Information**



**References**



**Citing Literature**



© 2018 AlphaMed Press  
STEM CELLS  
STEM CELLS Translational Medicine  
The Oncologist



AlphaMed Press | 318 Blackwell Street | Durham | NC | Contact Us

**About Wiley Online Library**

**Help & Support**

**Opportunities**

**Connect with Wiley**

Copyright © 1999-2018 John Wiley & Sons, Inc. All rights reserved





 About    Sections

